

# Response of the integrals in the Tremaine-Weinberg method to multiple pattern speeds: a counter-rotating inner bar in NGC 2950?

Witold Maciejewski

*Astrophysics, Denys Wilkinson Building, Keble Road, Oxford OX1 3RH*

## ABSTRACT

When integrals in the standard Tremaine-Weinberg method are evaluated for the case of a realistic model of a doubly barred galaxy, their modifications introduced by the second rotating pattern are in accord with what can be derived from a simple extension of that method, based on separation of tracer's density. This extension yields a qualitative argument that discriminates between prograde and retrograde inner bars. However, the estimate of the value of inner bar's pattern speed requires further assumptions. When this extension of the Tremaine-Weinberg method is applied to the recent observation of the doubly barred galaxy NGC 2950, it indicates that the inner bar there is counter-rotating, possibly with the pattern speed of  $-140 \pm 50 \text{ km s}^{-1} \text{ arcsec}^{-1}$ . The occurrence of counter-rotating inner bars can constrain theories of galaxy formation.

*Subject headings:* galaxies: individual (NGC 2950) — galaxies: kinematics and dynamics — galaxies: structure

## 1. Introduction

Bars within bars appear to be a common phenomenon in galaxies. Recent surveys indicate that up to 30% of early-type barred galaxies contain such double bars (Erwin & Sparke 2002; Laine et al. 2002). Inner bars remain distinct in near infrared (Wozniak et al. 1995), therefore fairly old stars must contribute to their light. The relative orientation of the two bars in doubly barred galaxies is random, therefore it is likely that the bars rotate with different pattern speeds.

The origin of multiply barred systems remains unclear. A bar takes away angular momentum from gas very efficiently, and in the young Universe bars might have been responsible for the early rapid growth of the massive black holes (Begelman, Volenteri & Rees 2006). If the innermost parts of galactic discs formed first, then early instabilities there might have lead to the formation of small-scale bars, which may be surviving in the present-day Universe as nuclear bars, often nested inside larger, outer bars, that might have formed later. Studying the dynamics of nested bars can therefore help us to understand the formation of galaxies and of their central massive black holes.

Our understanding of how double bars are sustained has significantly improved in the recent years. Maciejewski & Sparke (1997, 2000) have developed a formalism that enables finding families

of stable regular orbits in such systems. Stable regular orbits are robust structures, which define the shape of the galaxy, and therefore they can serve as a backbone for double bars. So far they have been analyzed for the case when the pattern speed of the inner bar is higher than that of the outer bar (Maciejewski & Sparke 2000). Using N-body simulations, Rautiainen et al. (2002) confirmed that stars get trapped around these orbits, and form long-lasting doubly barred systems. However, in this scenario the kinematics of the inner bar is not a scaled-down copy of that of the main bar, since the inner bar cannot extend to its corotation. Other numerical simulations have shown that systems of two counter-rotating bars are also possible (Sellwood & Merritt 1994; Friedli 1996), and systems with secondary bars rotating slower than the outer, main bars, have never been excluded on theoretical grounds.

Various dynamical scenarios for doubly barred galaxies may have different implications for the evolution of the galactic centres. In order to discriminate between them, one should measure the pattern speed of the inner bar. If only one pattern speed is present in the system, the Tremaine-Weinberg (1984) method allows to derive it using a set of simple kinematical measurements. Recent kinematical observations of the doubly barred galaxy NGC 2950 (Corsini, Debattista & Aguerri 2003; hereafter CDA03) are inconsistent with one pattern speed there. The observations are suggestive of another pattern speed in the area of the inner bar. CDA03 attempted to estimate it, but they concluded a wide range of values, consistent with a fast-rotating prograde secondary bar as well as with a retrograde one.

In this paper, I show that a simple extension of the Tremaine-Weinberg method to multiple pattern speeds, based on the separation of tracer’s density, is sufficient to discriminate between prograde and retrograde inner bars. Similar extension has been already considered by CDA03, but they disregarded it as not being rigorous enough. In Section 2, I examine in more detail the extended method, and I show that it immediately gives a qualitative information about the sign of rotation of the inner bar. In Section 3, I calculate the integrals in the original Tremaine-Weinberg method for the case of a realistic doubly barred galaxy, and I show that their departure from values for a single rotating pattern is the same as predicted by the extension to the Tremaine-Weinberg method proposed in Section 2. In Section 4, I examine one method to measure the pattern speed of the inner bar, and I show that it recovers the pattern speed in the model with an acceptable accuracy. When the extended Tremaine-Weinberg method proposed here is applied to NGC 2950, it indicates that the pattern speed of the inner bar there is smaller than the positive pattern speed of the outer bar, and that it is most likely negative (i.e. the inner bar is counter-rotating with respect to the outer bar and to the disc). The estimate of the pattern speed of the inner bar there is  $\Omega_S \simeq -140 \pm 50 \text{ km s}^{-1} \text{ arcsec}^{-1}$ . Limitations of the extended method, other attempts to estimate multiple pattern speeds using the Tremaine-Weinberg formalism, and consequences of counter-rotating inner bars for the evolution of galactic centres are discussed in Section 5.

## 2. A simple extension of the Tremaine-Weinberg method to multiple pattern speeds

The Tremaine-Weinberg method is designed for one pattern speed, which it derives from the centroid and the luminosity-weighted line-of-sight velocity of a chosen tracer moving in the galaxy's potential. The method rests on three assumptions: the disc of the galaxy is flat, it has a well-defined pattern speed, and the tracer obeys the continuity equation. Under these assumptions, the surface density of the tracer,  $\Sigma(x, y, t)$ , can be written as

$$\Sigma(x, y, t) = \tilde{\Sigma}(R, \varphi - \Omega_P t) \quad (1)$$

where  $\Omega_P$  is the pattern speed,  $(x, y)$  are Cartesian coordinates in the disc plane,  $(R, \varphi)$  are polar coordinates there, centred on the galactic centre, and  $t$  is time.

When another pattern speed is introduced, the two patterns cannot rotate rigidly one through another (Louis & Gerhardt 1988; Sridhar 1989; Maciejewski & Sparke 2000), and in principle one cannot split the right-hand side of (1) into components with different pattern speeds. However, let us assume that a rough separation of patterns is possible, and let us write, for a system with two pattern speeds  $\Omega_S$  and  $\Omega_B$ , the surface density of the tracer as

$$\Sigma(x, y, t) = \tilde{\Sigma}_B(R, \varphi - \Omega_B t) + \tilde{\Sigma}_S(R, \varphi - \Omega_S t) \quad (2)$$

Twofold interpretation of such a separation of tracer's density is possible. Either the tracer in the disc (e.g. stars) can be divided into subgroups belonging to two unchanging patterns, each rotating with a constant pattern speed, or one can separate radial zones in the galactic disc that rotate with constant pattern speeds, with no net exchange of the tracer between the zones. Neither of these interpretations is consistent with the dynamics of galaxies, because patterns rotating one through another change with time, and tracers of each pattern are often present at the same radius. However, if these inconsistencies are small, the separation (2) can still be approximately valid.

My approach is to limit the use of the extension of the Tremaine-Weinberg method based on the separation of tracer's density (2) to a qualitative prediction of how the integrals in the standard Tremaine-Weinberg method change when a second rotating pattern is introduced. In Section 3, I will show that this change, calculated properly for a realistic model of doubly barred galaxy, with bars oscillating in time, and with tracers of each bar overlapping, is the same as predicted by the extended method proposed here. Thus the separation of tracer's density may help in interpreting the Tremaine-Weinberg integrals in the models and in the observed galaxies.

Once tracer's density is separated according to (2), one can write two separate continuity equations. Further derivation is identical to the one performed by Tremaine & Weinberg (1984), and it can be conducted for each tracer's density separately, leading to two equations:

$$\Omega_B \sin i \int_{-\infty}^{+\infty} \Sigma_B(X, Y_{\text{slit}}) X dX = \int_{-\infty}^{+\infty} \Sigma_B(X, Y_{\text{slit}}) V_B^{\text{los}}(X, Y_{\text{slit}}) dX, \quad (3)$$

$$\Omega_S \sin i \int_{-\infty}^{+\infty} \Sigma_S(X, Y_{\text{slit}}) X dX = \int_{-\infty}^{+\infty} \Sigma_S(X, Y_{\text{slit}}) V_S^{\text{los}}(X, Y_{\text{slit}}) dX, \quad (4)$$

where  $(X, Y_{slit})$  are coordinates on the sky ( $X$  running parallel to the line of nodes and  $Y_{slit}$  being the offset, perpendicular to the line of nodes, of the slit along which the integration is performed),  $V^{los}$  is the observed line-of-sight velocity, and  $i$  is the inclination of the disc. Let the tracer be made of stellar-light emission; then one can define for each bar component, as well as for the whole galaxy the luminosity-density  $L_{\square} = \int_{-\infty}^{+\infty} \Sigma_{\square}(X, Y_{slit}) dX$ , the centroid  $X_{\square} = \frac{1}{L_{\square}} \int_{-\infty}^{+\infty} \Sigma_{\square}(X, Y_{slit}) X dX$ , and the luminosity-weighted line-of-sight velocity  $V_{\square} = \frac{1}{L_{\square}} \int_{-\infty}^{+\infty} \Sigma_{\square}(X, Y_{slit}) V_{\square}^{los}(X, Y_{slit}) dX$ , where the index  $\square$  is  $B$  for the outer bar,  $S$  for the inner bar, and  $tot$  for the whole galaxy. Obviously, only values with index  $tot$  can be observed, for example by placing a slit parallel to the line of nodes (Fig.1), and deriving along it the values of luminosity, centroid and line-of-sight velocity, where all integrals include integration over the width of the slit. With the definitions above, the sum of (3) and (4) takes a form

$$\Omega_B \sin i F_B X_B + \Omega_S \sin i F_S X_S = F_B V_B + F_S V_S, \quad (5)$$

where  $F_{\square} = L_{\square}/L_{tot}$ . CDA03 gave a similar equation, but in their convention there are no fractions  $F_{\square}$ . Note that equation (5) is not sufficient to derive two pattern speeds  $\Omega_{B,S}$  by measuring the centroid  $X_{tot}$  and the luminosity-weighted line-of-sight velocity  $V_{tot}$  along the slits. Although  $F_B V_B + F_S V_S \equiv V_{tot}$ , and it can be measured directly, the pattern speeds are combined with the unknown  $F_{B,S}$  and  $X_{B,S}$ .

However, the form of equation (5), together with the morphology of the doubly barred galaxy, whose pattern speeds we want to measure, already reveals some information about the relation between the two pattern speeds. The line of nodes passing through the centre of the galaxy sets a division of this galaxy into four quadrants. Consider for example the case when the two bars lie in opposite quadrants of the galaxy (Fig.1). This is the case of NGC 2950. Even if we cannot measure  $X_B$  or  $X_S$ , we know that they are always of opposite signs, no matter how the slit is placed (parallel to the line of nodes). Then if  $\Omega_B$  and  $\Omega_S$  are of the same sign, adding the inner bar should bring the sum on the left of (5) closer to zero (or even through zero for strong fast inner bars) when compared to the contribution of the outer bar alone. This implies that the observed  $|V_{tot}|$  should be smaller when entering the region of the inner bar than that interpolated from the outer bar. To the contrary, CDA03 observe  $|V_{tot}|$  *increasing* around this transition region in NGC 2950, consistent with  $\Omega_S$  having the sign opposite to  $\Omega_B$ , i.e. with the counter-rotating secondary bar.

### 2.1. Immediate condition for the sign of $\Omega_S - \Omega_B$

In the argument above, no reference point has been fixed, since the sums on each side of (5) get modified by the introduction of the secondary bar. We do not know the contribution from the outer bar in the region where the inner bar is present, and interpolation can be misleading. Here I show that equation (5) allows to tell whether  $\Omega_S > \Omega_B$  or  $\Omega_S < \Omega_B$ . Equation (5) can be rewritten as

$$\Omega_B X_{tot} + X_S F_S (\Omega_S - \Omega_B) = V_{tot} / \sin i. \quad (6)$$

This form shows how the relation between the integrals  $V_{tot}$  and  $X_{tot}$  gets modified by the presence of the secondary bar: the second term in the sum is a correction term. For slits outside the inner bar this correction is zero (because  $\Sigma_S$  is zero there), and for those slits the observed values of  $X_{tot}$  and  $V_{tot}$  should lie on a straight line of inclination  $\Omega_B \sin i$ . When the slit passes through the inner bar,  $X_S \neq 0$ . If for such slits  $|V_{tot}|$  is larger than the values given by the linear relation (6) without the correction factor, then the correction has to have the same sign as  $\Omega_B X_{tot}$ . For the bars that lie in opposite quadrants, like in NGC 2950 (Fig.1),  $X_B$  and  $X_S$  are of opposite signs, and  $X_{tot}$  has the same sign as  $X_B$  throughout the galaxy (CDA03, fig.3). Therefore the two components of the sum in (6) can only be of the same sign when  $\Omega_B$  has opposite sign to  $\Omega_S - \Omega_B$ . If we take a convention that  $\Omega_B > 0$  then  $\Omega_S < \Omega_B$ .

This argument can be extended to the case when  $X_{tot}$  changes sign for slits passing through the secondary bar. In NGC 2950, the values of  $X_{tot}$  for these slits are very small, which is consistent with the observed geometry of bars. A similar argument can be applied to galaxies with bars in the same quadrants, where  $X_{tot}$  for innermost slits is not that small. In this case,  $X_B$ ,  $X_S$  and  $X_{tot}$  are all of the same sign. If an increase of  $|V_{tot}|$  is observed in the region of the inner bar,  $\Omega_B$  must now have the same sign as  $\Omega_S - \Omega_B$ , which means  $\Omega_S > \Omega_B$  for the assumed  $\Omega_B > 0$ . Thus we see that the same increase of  $|V_{tot}|$  in the region of the inner bar can either indicate the inner bar rotating slower or faster than the outer bar, depending on the relative orientation of the bars.

## 2.2. Condition for counter-rotation

In some cases, an argument can be made about corotation or counter-rotation of the inner bar with respect to the inertial frame. It relies on the variation of the integrals in the Tremaine-Weinberg method with the distance of the slit from the centre of the galaxy,  $Y_{slit}$ . This argument can be made under an assumption that  $|X_B F_B|$  does not increase when we march with the slit through the galaxy toward the line of nodes (in the direction marked by an arrow on the left of Fig.1). This is a justified assumption, since  $F_B$  decreases inward for the very reason of the introduction of the secondary bar, and  $|X_B|$  should not go up inward, since early-type galaxies like NGC 2950 have 'flat' bars with a nearly constant surface brightness as a function of radius (Elmegreen et al. 1996).

Consider again equation (5). Normally, for slits that avoid the secondary bar,  $|V_{tot}|$  decreases inward (i.e. when shifting the slit in the direction given by the arrow in Fig.1). This is also the case in NGC 2950 (CDA03, fig.3). If then  $|V_{tot}|$  increases inward when the slit reaches the secondary bar (like in NGC 2950), this can be caused by either of the two components of the sum on the left of (5). I already argued that the first component cannot be the cause, since  $F_B$  decreases,  $|X_B|$  is unlikely to increase, and  $\Omega_B = \text{const}$ . The second component can only cause the increase of the sum when it is of the same sign as the first one. But again,  $X_B$  and  $X_S$  are of opposite sign. Therefore  $\Omega_S$  and  $\Omega_B$  have to be of opposite sign, too.

One can repeat this reasoning for a galaxy with bars in the same quadrants, to show that in that case  $|V_{tot}|$  increasing in the region of the inner bar indicates that the inner bar is corotating in the inertial frame. Similarly to the previous subsection, the conclusion about the pattern speed of the inner bar depends on the relative orientation of the bars.

### 3. Integrals in the Tremaine-Weinberg method calculated for a realistic model of a doubly barred galaxy

Regular motion of a particle in a potential of a doubly barred galaxy has two frequencies associated with it, each related to one of the bars, in addition to the frequency of its free oscillations (Maciejewski & Sparke 1997). In the linear approximation this motion corresponds to epicyclic oscillations with these frequencies around the guiding radius. Particles with the same guiding radii are bound to closed curves (loops) that oscillate in the pulsating potential of double bars. Loops are also observed in nonlinear analysis (Maciejewski & Sparke 2000; Maciejewski & Athanassoula 2006).

The orbital approach directly indicates that the motion of a particle associated with one bar has always a component coming from the other bar. Amplitudes of the oscillations can be easily evaluated in the linear approximation (Maciejewski 2003), giving particle's position and velocity at each relative position of the bars. In Figure 2, I plot the loops populated by particles moving in the potential of a doubly barred galaxy constructed by Maciejewski & Sparke (2000; Model 2). This is a realistic potential, since it admits orbits that support the outer bar, as well as orbits supporting the inner bar, throughout the extent of each bar. The two bars in this model rotate in the same direction with pattern speeds  $\Omega_B = 35 \text{ km s}^{-1} \text{ kpc}^{-1}$  and  $\Omega_S = 110 \text{ km s}^{-1} \text{ kpc}^{-1}$ . I plot the loops for two relative orientations of the bars: the bars parallel (Fig.2, left), and the bars at the angle of 112.5 degrees, the value similar to that observed in NGC 2950 after deprojection (Fig.2, right). The loops change shapes as the bars rotate one with respect to another, and loops associated with one bar intersect the loops associated with the other bar. Thus formally one cannot perform here the separation of tracer's density postulated in (2).

However, changes in the shapes of the bars, and zones where both tracers coexist, may be small, and then what formally prohibits the separation may turn into a higher-order correction to it. In order to check whether it is the case for the realistic Model 2 (Maciejewski & Sparke 2000), I calculated the positions and velocities of some  $10^6$  points on 200 loops in this model, from which I obtained the luminosity-weighted positions  $X_{tot}$  and the line-of-sight velocities  $V_{tot}$  along slits placed at the same relative angle to the outer bar as in the CDA03 observations of NGC 2950 (dotted straight lines in Fig.2). In the model, I use deprojected velocities, which replaces  $V_{tot}/\sin i$  by  $V_{tot}$ , and I measure  $Y_{slit}$  in the plane of the galaxy.

In the left panel of Figure 3, I plot the value of the centroid,  $X_{tot}$ , as a function of the offset of the slit from the galaxy centre,  $Y_{slit}$ . When the inner bar is placed at the position similar to

the one observed in NGC 2950, the value of  $X_{tot}$  (solid line) is closer to zero in the region of the inner bar ( $|Y_{slit}| < 1$ ), than when the inner bar is absent (dot-dashed line). However,  $X_{tot}$  does not change the sign in the region of the inner bar, which is also observed in NGC 2950 (CDA03, fig.3b). This indicates that the light integrated along a slit passing through the inner bar is still dominated by the outer bar. In the case of the two bars parallel (Fig.2, left panel) there is no such decrease of  $X_{tot}$  in the region of the inner bar (dashed line in Fig.3, left panel).

In the central panel of Figure 3, I plot the luminosity-weighted line-of-sight velocity,  $V_{tot}$ , as a function of the same offset of the slit from the galaxy centre,  $Y_{slit}$ , as in the left panel of Figure 3. When the inner bar, rotating in the same direction as the outer bar, but faster, is placed at the position similar to the one observed in NGC 2950, the value of  $V_{tot}$  (solid line) rapidly approaches zero in the region of the inner bar ( $|Y_{slit}| < 1$ ), and in most of this region it has the sign opposite to the value of  $V_{tot}$  for slits not passing through the inner bar ( $|Y_{slit}| > 1$ ). This behaviour of  $V_{tot}$  is opposite to that observed in NGC 2950 by CDA03. For the model of galaxy with  $\Omega_S > \Omega_B$ , changes of  $V_{tot}$  with  $Y_{slit}$  observed by CDA03 can only be reproduced when both bars lie in the same quadrants of the galaxy. For the particular case of bars parallel, presented here,  $|V_{tot}|$  increases in the region of the inner bar (dashed line in Fig.3, central panel), relative to the case when there is no inner bar (dot-dashed line). This dependence of departures in  $V_{tot}$  on the relative position of the two bars is exactly as expected from the simple extension of the Tremaine-Weinberg method derived Section 2, based on the separation of tracer's density (2). Namely, if the inner bar rotates faster than the outer bar then, when both bars are in the same quadrants (defined by the line of nodes and the centre of the galaxy),  $|V_{tot}|$  increases in the slits passing through the inner bar, but it *decreases*, when the bars are in the opposite quadrants.

The plot of  $V_{tot}$  as a function of  $X_{tot}$  is presented in the right panel of Figure 3. One may attempt to fit a second straight line in the region of the inner bar, but this fit will not reproduce the actual pattern speed of the inner bar. In Figure 4, I plot the ratios of  $V_{tot}/X_{tot}$  as estimators of the derived  $\Omega_{pattern}$ . For a single bar (dot-dashed line), there is one pattern speed independent of the offset of the slit, and equal to the one assumed in the model. If there are two pattern speeds in the system, the inner bar does not alter significantly the pattern speed of the outer bar derived from the slits that do not pass through this inner bar. However, the induced departures are systematic: pattern speed of the outer bar is spuriously increased when the bars lie in the same quadrants, and decreased when they lie in quadrants opposite. The effect is small though, below 10%.

If the bars lie in opposite quadrants (solid line), the derived  $\Omega_{pattern}$  rapidly decreases for the slit passing through the inner bar, and it becomes negative, not giving any information about the pattern speed of the inner bar. If the bars lie in the same quadrants (dashed line), the derived  $\Omega_{pattern}$  is larger than  $\Omega_B$  for the slits passing through the inner bar, but it varies with  $Y_{slit}$ , and never reaches the value of  $\Omega_S = 110 \text{ km s}^{-1} \text{ kpc}^{-1}$  assumed in the model, remaining at slightly over half of that value.

#### 4. A method to derive the value of $\Omega_S$

The main goal of this paper is to show that with a simple extension of the Tremaine-Weinberg method to multiple pattern speeds one can derive at least rough qualitative information about the secondary pattern rotation. For the data on NGC 2950 presented by CDA03 this information is that the inner bar rotates in the opposite direction than the outer bar. On the other hand, getting the numerical value of the pattern speed of the secondary bar,  $\Omega_S$ , may not be possible without making additional assumptions. Here I analyse one possible method to calculate  $\Omega_S$ .

If the tracer of the secondary bar does not extend beyond some radius  $R_0$  in the galaxy plane (outlined in projection by the dotted ellipse in Fig.1), then (4) can be rewritten as

$$\Omega_S \sin i \int_{-X_0}^{X_0} \Sigma_S(X, Y_{\text{slit}}) X dX = \int_{-X_0}^{+X_0} \Sigma_S(X, Y_{\text{slit}}) V_S^{\text{los}}(X, Y_{\text{slit}}) dX, \quad (7)$$

where  $R_0^2 = (Y_{\text{slit}}/\cos i)^2 + X_0^2$ . Summing (3) and (7) leads to

$$\Omega_B X_{\text{tot}} + L_{\text{tot}}^{-1}(\Omega_S - \Omega_B) \int_{-X_0}^{X_0} \Sigma_S(X, Y_{\text{slit}}) X dX = V_{\text{tot}}/\sin i. \quad (8)$$

However, aside for  $\Omega_S$ , we still do not know the integral in (8). It can be approximated when one assumes that only tracers of the inner bar and of the axisymmetric component are present inside the dotted ellipse in Figure 1, i.e. that the outer bar is almost axisymmetric in this region. Note that this is a strong and poorly founded assumption. However, if we take it, and since the contribution of the axisymmetric component to the integral in (8) cancels out, one can substitute there the observable  $\Sigma_{\text{tot}}$  for the unknown  $\Sigma_S$ , and rewrite (8) as a linear regression of  $\Omega_S - \Omega_B$ :

$$(\Omega_S - \Omega_B) \frac{1}{L_{\text{tot}}} \int_{-X_0}^{X_0} \Sigma_{\text{tot}}(X, Y_{\text{slit}}) X dX = V_{\text{tot}}/\sin i - \Omega_B X_{\text{tot}}. \quad (9)$$

Thus  $\Omega_S - \Omega_B$  can be obtained as a slope of a straight line fitted to the data from slits passing through the inner bar. A similar equation has been used by CDA03 to estimate  $\Omega_S$ , but here the coefficient at  $\Omega_S - \Omega_B$  is defined differently.

I tested equation (9) on the model examined in Section 3, for the position angles of the bars like the ones observed in NGC 2950. On the basis of the shapes of the loops, I chose  $R_0 = 1.1$  kpc for this model, and I used  $\Omega_B = 35 \text{ km s}^{-1} \text{ kpc}^{-1}$ . In Figure 5, I plot the data points for the regression (9). They follow a straight line well, except for the points around zero values. However, these points come from  $Y_{\text{slit}} \simeq R_0$ , where the integration is over a small number of particles, hence random error is large there. If we exclude these points, the derived  $\Omega_S - \Omega_B$  oscillates between 60 and 70  $\text{km s}^{-1} \text{ kpc}^{-1}$  for  $|Y_{\text{slit}}| < 0.75$  kpc. This gives  $\Omega_S$  between 95 and 105  $\text{km s}^{-1} \text{ kpc}^{-1}$ , consistent with the input value of 110  $\text{km s}^{-1} \text{ kpc}^{-1}$ , with an error of about 10%.

In order to apply the same method to the observed data on NGC 2950 from CDA03, the value of  $R_0$  can be estimated by checking how the integral in (9) changes with varying  $R_0$  — it should

have a plateau in the transition area between the bars. I used the R-band image of NGC 2950 (Erwin & Sparke 2003) to calculate this integral and  $L_{tot}$  for each of the slits passing through the secondary bar, placed at positions reported by CDA03. The values of  $\frac{1}{L_{tot}} \int_{-X_0}^{X_0} \Sigma_{tot}(X, Y_{slit}) X dX$  as a function of  $R_0$  are plotted in Figure 6. All curves indeed have a plateau around the same  $R_0$  of 5–6 arcsec. It is located just outside a nuclear stellar ring at  $\sim 4.2$  arcsec, reported by Erwin & Sparke (2003), which is likely circular in the plane of the galaxy. Thus the method proposed here may be particularly well suited for NGC 2950.

Each curve in Figure 6 has a characteristic U-shape, whose depth depends on the relative contribution of the inner bar to the integral in (9), and therefore it vanishes outside the inner bar, and also very close to the line of nodes, where the integral tends to be zero. From the R-band image, the depth is largest for slits offset by  $\sim \pm 1$  arcsec. The linear fit to (9), with the data for  $V_{tot}$  and  $X_{tot}$  from each slit passing through the inner bar provided by CDA03, reveals a large negative value of  $\Omega_S - \Omega_B$ , about  $-150 \pm 50$  km s $^{-1}$  arcsec $^{-1}$ . For  $\Omega_B \simeq 11$  km s $^{-1}$  arcsec $^{-1}$ , measured by CDA03, this gives  $\Omega_S \simeq -140 \pm 50$  km s $^{-1}$  arcsec $^{-1}$ . This result, although with much poorer grounds than the qualitative arguments from Section 2, reaffirms counter-rotation of the inner bar. Note that the unrealistically large value of  $\Omega_S$  derived with this method is likely an overestimate: in order to get it, the integral  $\int_{-X_0}^{X_0} \Sigma_{tot}(X, Y_{slit}) X dX$  has been substituted for  $\int_{-X_0}^{X_0} \Sigma_S(X, Y_{slit}) X dX$ . The substituted integral is most likely smaller than the original one, because the contributions of the two bars are of opposite signs.

## 5. Discussion

It is interesting to note that although the original Tremaine-Weinberg method has been derived under stringent assumptions, it has been recently used successfully in analyses that explicitly break one or more of its assumptions (e.g. Zimmer, Rand & McGraw 2004, Hernandez et al. 2005). It shows that this method is surprisingly robust. Often tracers are being used, for which the continuity equation is violated. In the extension to the Tremaine-Weinberg method proposed here, the tracer fulfills the continuity equation globally. However, continuity may be violated for the separation of tracer's surface density proposed in (2), when stars are allowed to transfer from following one bar to the other. This effect should be small though, since in self-consistent models of double bars, orbits that are trapped and oscillate around one or the other bar, populate large fraction of phase space (Maciejewski & Sparke 2000; Maciejewski & Athanassoula 2006). Similarly, other effects that for multiple pattern speeds formally prohibit separation of the tracer's surface density proposed in (2), are likely to play a small role, as indicated by the analysis of a realistic doubly barred galactic potential. Namely, even if each particle in the system oscillates with frequencies related to both bars, for most of the particles one frequency dominates, and the separation can be performed. The radial separation of the tracers, necessary for the estimate of the pattern speed of the inner bar in Section 4, can also be possible if the zones, where tracers with each of the two patterns coexist, occupy small fraction of the galaxy. The larger this fraction, the poorer is the estimate of the inner

bar's pattern speed.

This paper shows that the change in value of the integrals  $X_{tot}$  and  $V_{tot}$  in the original Tremaine-Weinberg formalism, caused by the second pattern speed, depends on the relative position of the bars. In particular, I showed that fitting another straight line in the  $X_{tot} - V_{tot}$  diagram to the data from slits passing through the inner bar *does not* yield the pattern speed of this bar. Therefore recent derivations of multiple pattern speeds based on such analysis (Rand & Wallin 2004; Hernandez et al. 2005) have to be treated with caution.

The retrograde rotation of the inner bar in NGC 2950 proposed here is inconsistent with the first estimate of  $\Omega_S$  by CDA03. However, in that estimate it is assumed that the inner bar dominates light in the slits passing through it. This cannot be correct, since  $X_{tot}$  and  $X_S$  are of opposite sign there, which indicates that the light from the outer bar still dominates the slits passing through the inner bar. The second estimate of CDA03, like the estimate given in this paper, indicates that the inner bar is counter-rotating.

The obvious next step in verifying counter-rotation of the inner bar in NGC 2950 would be an examination of orbital structure of a galaxy with a retrograde inner bar, following the method presented in Section 3. However, a bar counter-rotating with respect to its stellar disc has to be built out of so called  $x_4$  orbits, which are normally very close to circular (see e.g. Sellwood & Wilkinson 1993). In terms of the linear approximation of Section 3, the amplitude of oscillation around the guiding radius generated by a retrograde bar is very small (see equations (12) and (13) in Maciejewski 2003). Thus a construction of a retrograde bar in a prograde stellar disc is unlikely. This is consistent with N-body simulations, in which multiple pattern speeds form naturally in stellar discs (Rautiainen et al. 2002) — these simulations do not recover retrograde pattern speeds.

This leads to another possibility, namely that the inner bar is formed out of an inner disc that counter-rotates with respect to the outer disc. Numerical results indicate that two counter-rotating bars, formed in two counter-rotating stellar discs that overlap each other, can survive in galaxies for many rotation periods (Sellwood & Merritt 1994; Friedli 1996). If this is the case, one should find out whether a retrograde inner disc is consistent with the rotation curve and velocity dispersion in NGC 2950. The data presented by CDA03 do not indicate counter-rotation in the innermost few arc-seconds of NGC 2950.

If further kinematical studies of NGC 2950 confirm counter-rotation in its innermost parts, then extending the Tremaine-Weinberg method along the lines proposed here may yield an efficient way of detecting counter-rotation in galaxies with nested bars. The fraction of counter-rotating inner bars can constrain theories of galaxies formation and evolution. Currently the most accepted view on the origin of the inner bar is that it forms through instabilities in gas inflowing along the outer bar (Shlosman, Frank & Begelman 1989). However, if inner bars form on early stages of galaxy assembling, and outer bars form from material that settled on the galaxy later, the spins of the two bars may be unrelated, leading to a large fraction of counter-rotating inner bars. Determining this fraction may help to distinguish between these two evolutionary scenarios.

## 6. Conclusions

In this paper I presented an argument that a simple extension of the Tremaine-Weinberg method to multiple pattern speeds can provide an information about the sense of rotation of the inner bar in doubly barred galaxies. The extended formula advocated here links the relative position of the bars to the sign of rotation of the inner bar. Although this extension cannot be as rigorous as the original method, it predicts the same departures of the integrals in the Tremaine-Weinberg method from their values for the single rotating pattern, as in the orbital model of a doubly barred galaxy, even if this model explicitly violates the assumptions underlying this extension. This is likely because the effects of violation of these assumptions are small, and they do not alter significantly the basic results.

If these assumptions are not severely violated in NGC 2950, then the inner bar there counter-rotates with respect to the outer bar and to the large-scale disc. Since a retrograde bar is unlikely to be supported in a prograde disc, a retrograde inner disc may be hiding in the central kiloparsecs of NGC 2950.

I wish to thank Peter Erwin for letting me use the R-band image of NGC 2950, which he obtained with the WYIN telescope. I am grateful to the authors of the CDA03 paper for sharing the details of their observations with me. Discussions with Linda Sparke improved presentation of this argument. This work was partially supported by the Polish Committee for Scientific Research as a research project 1 P03D 007 26 in the years 2004–2006.

## REFERENCES

Begelman M.C., Volonteri M., Rees M.J., 2006, astro-ph/0602363

Corsini E.M., Debattista V.P., Aguerri J.A.L., 2003, ApJ, 599, L29

Elmegreen D.M., Elmegreen B.G., Chromei F.R., Hasselbacher D.A., Bissel B.A., 1996, AJ, 111, 2233

Erwin P., Sparke, L.S., 2002, AJ, 124, 65

Erwin P., Sparke, L.S., 2003, ApJS, 146, 299

Friedli D., 1996, A&A, 312, 761

Hernandez O., Wozniak H., Carignan C., Amram P., Chemin L., Daigle O., 2005, ApJ, 632, 253

Laine S., Shlosman I., Knapen J.H., Peletier, R.F., 2002, ApJ, 567, 97

Louis P.D., Gerhard O.E., 1988, MNRAS, 233, 337

Maciejewski W., 2003, in: Contopoulos G., Voglis N. (eds.) Lecture Notes in Physics Vol. 626, Springer Verlag, Berlin, 91

Maciejewski W., Athanassoula E., 2006, in preparation

Maciejewski W., Sparke L.S., 1997, *ApJ*, 484, L117

Maciejewski W., Sparke L.S., 2000, *MNRAS*, 313, 745

Rautiainen P., Salo H., Laurikainen E., 2002, *MNRAS*, 337, 1233

Rand R.J., Wallin J.F., 2004, *ApJ*, 614, 142

Sellwood J. A., Merritt, D., 1994, *ApJ*, 425, 530

Sellwood J. A., Wilkinson A., 1993, *Rep. Prog. Phys.*, 56, 173

Shlosman I., Frank J., Begelman M.C., 1989, *Nature*, 338, 45

Sridhar S., 1989, *MNRAS*, 238, 1159

Tremaine S., Weinberg M.D., 1984, *ApJ*, 282, L5

Wozniak H., Friedli D., Martinet L., Martin P., Bratschi P., 1995, *A&AS*, 111, 115

Zimmer P., Rand R.J., McGraw J.T., 2004, *ApJ*, 607, 285

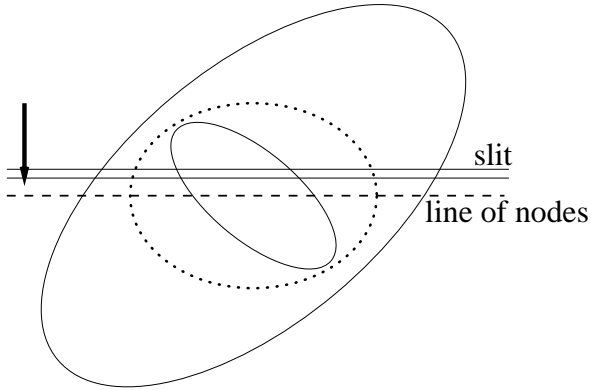


Fig. 1.— Schematic drawing of the positions of the bars observed in NGC 2950 and of an exemplary location of the slit. Two solid ellipses outline the bars, and the dotted ellipse marks the boundary used in the derivation in Section 4.

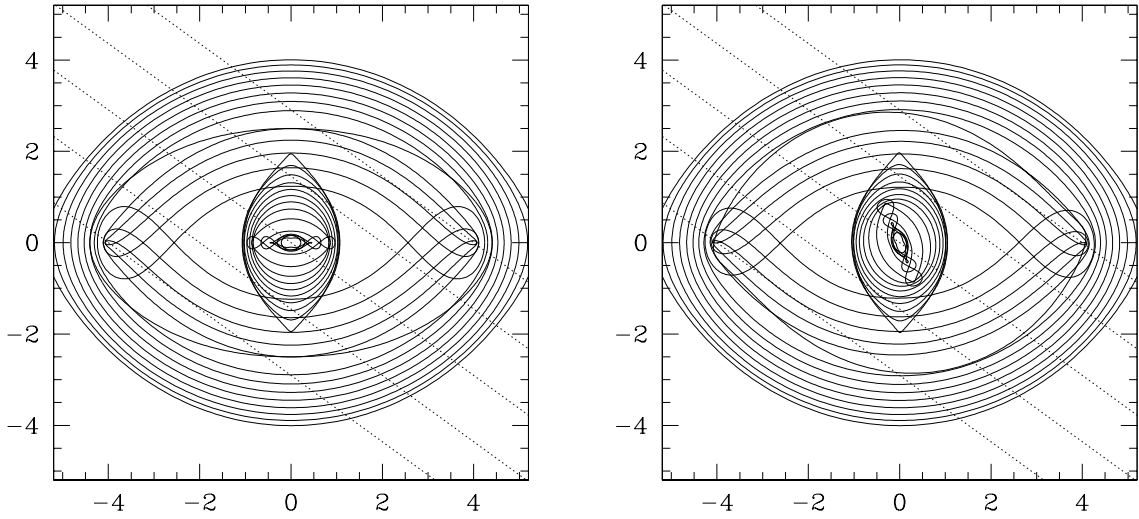


Fig. 2.— Loops in a realistic model of doubly barred galaxy (Model 2 of Maciejewski & Sparke 2000) in the linear approximation. Dashed lines mark the direction along which 'slits' are placed, for which the integrated values of  $X_{tot}$  and  $V_{tot}$  are derived. The bars are aligned in the left panel, and at  $112.5^\circ$  angle in the right panel. Units on axes are in kpc.

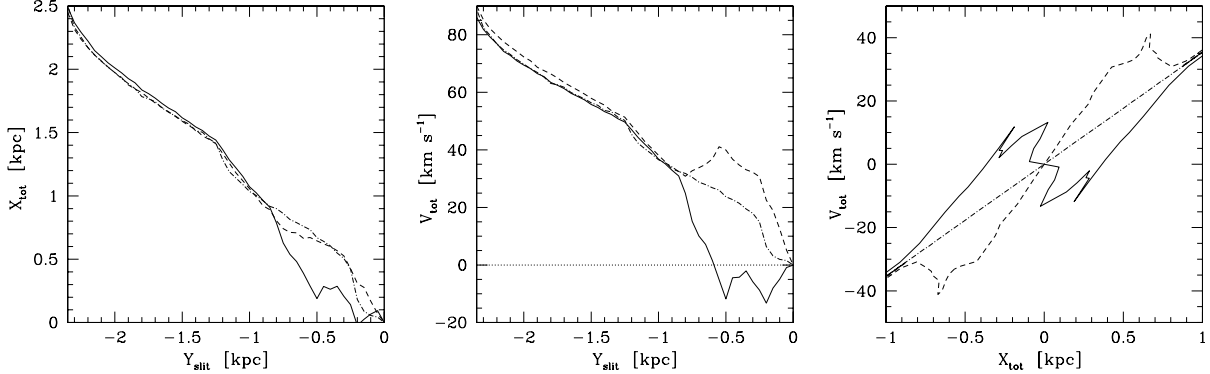


Fig. 3.— Values of the integrals in the Tremaine-Weinberg method, calculated from the epicyclic formulae for the positions and velocities of particles in the realistic model of doubly barred galaxy from Figure 2. The dot-dashed line corresponds to the model without the inner bar, the dashed line is for the model with two bars aligned, as in the left panel of Figure 2, while the solid line is for the model with two bars located as in the right panel of Figure 2. This figure can be directly compared with fig.3 in CDA03. *Left:* The photometric integrals  $X_{tot}$ , defined in Section 2, as a function of the slit offset  $Y_{slit}$  with respect to the centre of the galaxy. *Centre:* The kinematic integrals  $V_{tot}$ , defined in Section 2, as a function of the slit offset  $Y_{slit}$ . *Right:*  $V_{tot}$  as a function of  $X_{tot}$ .

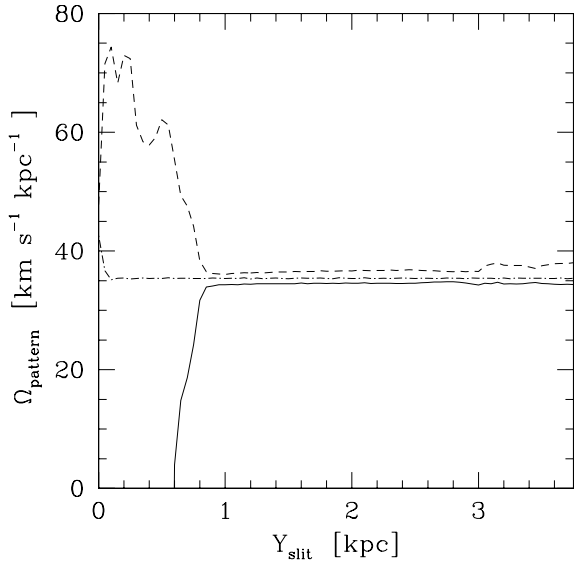


Fig. 4.— Pattern speed in the model,  $\Omega_{pattern} \equiv V_{tot}/X_{tot}$ , derived separately for each position of the slit  $Y_{slit}$ . Correspondence of line types is the same as in Figure 3.

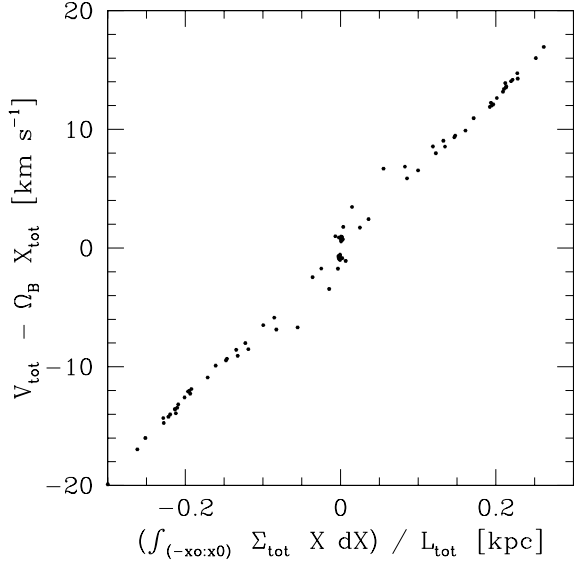


Fig. 5.— Model values of the integrals that determine the linear regression in (9) with the expected slope of  $\Omega_S - \Omega_B$ . Values of  $\frac{1}{L_{tot}} \int_{-X_0}^{X_0} \Sigma_{tot}(X, Y_{slit}) X dX$  are plotted against  $V_{tot} - \Omega_B X_{tot}$ .

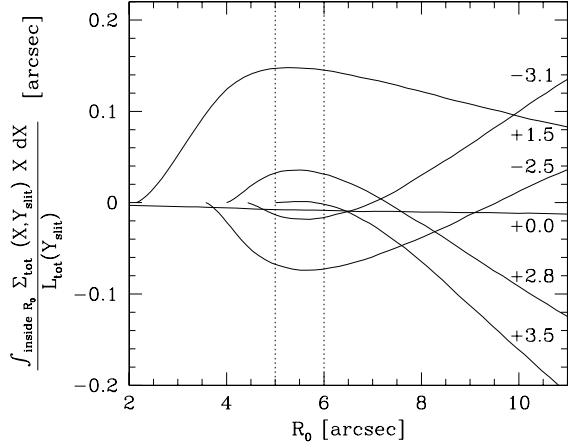


Fig. 6.— Values of  $\frac{1}{L_{tot}} \int_{-X_0}^{X_0} \Sigma_{tot}(X, Y_{slit}) X dX$  as a function of  $R_0 = \sqrt{(Y_{slit}/\cos i)^2 + X_0^2}$  for NGC 2950. The curves are derived from the R-band image of NGC 2950 (Erwin & Sparke 2003), for slits placed parallel to the line of nodes, and offset from it by values given on the right of the plot in arcsec. Two dotted vertical lines indicate a plateau range, common for all the curves.